SEDIMENTOLOGY the journal of the International Association of Sedimentologists

Sedimentology (2015) doi: 10.1111/sed.12236

Response of low-angle dunes to variable flow

MEGAN L. HENDERSHOT*†, JEREMY G. VENDITTI*, RYAN W. BRADLEY*, RAY A. KOSTASCHUK*, MICHAEL CHURCH‡ and MEAD A. ALLISON§¶
*Department of Geography, Simon Fraser University, Burnaby, BC, Canada V5A 1S6 (E-mail: jeremy_venditti@sfu.ca)
‡Department of Geography, The University of British Columbia, Vancouver, BC, Canada V6T 1Z2
§The Water Institute of the Gulf, Baton Rouge, LA 70825, USA
¶Department of Earth & Environmental Sciences, Tulane University, New Orleans, LA 70118, USA

Associate Editor – Vern Manville

ABSTRACT

Current understanding of bedform dynamics is largely based on field and laboratory observations of bedforms in steady flow environments. There are relatively few investigations of bedforms in flows dominated by unsteadiness associated with rapidly changing flows or tides. As a consequence, the ability to predict bedform response to variable flow is rudimentary. Using high-resolution multibeam bathymetric data, this study explores the dynamics of a dune field developed by tidally modulated, fluvially dominated flow in the Fraser River Estuary, British Columbia, Canada. The dunes were dominantly low lee angle features characteristic of large, deep river channels. Data were collected over a field *ca* 1·0 km long and 0·5 km wide through a complete diurnal tidal cycle during the rising limb of the hydrograph immediately prior to peak freshet, yielding the most comprehensive characterization of low-angle dunes ever reported. The data show that bedform height and lee angle slope respond to variable flow by declining as the tide ebbs, then increasing as the tide rises and the flow velocities decrease. Bedform lengths do not appear to respond to the changes in velocity caused by the tides. Changes in the bedform height and lee angle have a counterclockwise hysteresis with mean flow velocity, indicating that changes in the bedform geometry lag changes in the flow. The data reveal that lee angle slope responds directly to suspended sediment concentration, supporting previous speculation that low-angle dune morphology is maintained by erosion of the dune stoss and crest at high flow, and deposition of that material in the dune trough.

Keywords Low-angle dunes, symmetrical dunes, tidally influenced flows, unsteady flow bedforms.

INTRODUCTION

In sedimentary systems, interdependence exists among fluid flow, deposit morphology and sediment transport (Leeder, 1983). In rivers, the topography of the channel bed influences the overlying flow field, while the interaction of the flow field with the labile bed gives rise to bedforms by means of sediment transport, resulting in a large-scale coupling that has been considered in the literature as far back as Sorby (1852, 1908). In sand-bedded rivers, the most common bedforms are dunes (Venditti, 2013). The morphodynamics of dunes play an important role in the transport of bed material and can add significant flow resistance in a

†Present address: Environment and Water, SNC Lavalin, Kelowna, BC, Canada V1Y 2E1.

channel. Geometric properties of a dune, such as height (*H*), length (*L*), aspect ratio (*H/L*) and stoss and lee slope angles (θ_{Stoss}, θ_{Lee}, respectively), are functions of the nature of dune growth, diminution, and migration through erosion and deposition of sediment associated with variable flows.

Dune dimensions have been linked to boundary layer thickness (Allen, 1968; Ashley, 1990; Southard & Boguchwal, 1990a,b) which, in rivers, is limited by depth of flow (*h*). Empirical correlations show that an increase in depth increases dune dimensions (e.g. Allen, 1982). Relative dune height (*H/h*) has been observed to range between 1/40 and 1/2·5, while the relative wavelength of a dune (*L/h*) has been found to lie between 1 and 16 (Allen, 1982; Venditti, 2013). These ratios translate to typical ranges of order 10^{-1} to 10^{1} m in height and order 10^{0} to 10^{2} m in length.

Dunes have been classified on the basis of stream-wise profile, as high-angle dunes (HADs) or low-angle dunes (LADs) (Kostaschuk & Villard, 1996, 1999; Venditti, 2013). High-angle dunes are asymmetrical in profile with long, gently sloping stoss sides and short, steep angle of repose lee slopes of *ca* 30°. Low-angle dunes have lee angles lower than the angle of repose, frequently less than 10°, with stoss and lee sides of comparable lengths, and hence more symmetrical profiles. High-angle dunes are found primarily in laboratory flumes and shallow rivers (e.g. Venditti & Bauer, 2005). Flow over a HAD converges and accelerates as it moves up the stoss side of the dune and separates at the dune crest to form a zone of reversed (upstream) flow and a turbulent wake region that propagates downstream (e.g. Wiberg & Nelson, 1992; Lyn, 1993; Nelson *et al.*, 1993; McLean *et al.*, 1994; Bennett & Best, 1995; Venditti & Bennett, 2000; Coleman *et al.*, 2006; Fernandez *et al.*, 2006; Paarlberg *et al.*, 2007; Venditti, 2007). Low-angle dunes are the predominant bedform in large, deep rivers and estuaries (e.g. Kostaschuk & Ilersich, 1995; Kostaschuk & Villard, 1996, 1999; Roden, 1998; ten Brinke *et al.*, 1999; Best & Kostaschuk, 2002; Nittrouer *et al.*, 2008; Shugar *et al.*, 2010; Bradley *et al.*, 2013). Scale model (Best & Kostaschuk, 2002) and field (e.g. Kostaschuk & Villard, 1996; Holmes & Garcia, 2008; Kostaschuk *et al.*, 2009; Bradley *et al.*, 2013) measurements of flow over LADs have demonstrated that, in contrast to HADs, flow separation downstream of the crest is intermittent or even non-existent, and is characterized by a zone of convergent accelerating flow up the stoss slope and a zone of divergent deceleration down the lee slope owing to topographic forcing. As far as the present authors are aware, LADs have never been generated in flumes.

Transport stage exerts an important control on dune shape: field studies (Smith & McLean, 1977; Soulsby *et al.*, 1991), laboratory experiments (Johns *et al.*, 1990) and theoretical analysis (Kostaschuk & Best, 2005) have suggested that, where suspended sediment transport of bed material dominates, LADs are common, and where bedload transport is dominant, the classic HAD shape is more common (Kostaschuk, 2006). Flume experiments by Yalin (1972) and Yalin & Karahan (1979) showed that *H/L* increases with transport stage from bedload-dominated through the mixed load regime, and then declines as the transport stage increases to suspended sediment domination. Observations in flumes (e.g. Allen, 1985) show that the steep lee angle of HADs is maintained by 'avalanching' of bedload that accumulates at the top of the lee slope and generates shallow sand flows down the lee. Field measurements over LADs (e.g. Kostaschuk, 2005) suggest that deposition of suspended sand in the trough and on the lower lee slope may result in lower lee slope angles.

While the geometry and dynamics of bedforms in steady flow environments such as rivers have been well-documented, much of the work has been limited to single track surveys, small-scale flume investigations or simplified modelling. There is a lack of high-resolution bed topography in three-dimensional (3D) dune fields under variable flow and on a larger physical scale than available in flume experiments. As a consequence, the current ability to predict bedform dynamics in variable flow environments such as tidally influenced rivers and estuaries remains poor. Observations from tidally influenced rivers and estuaries suggest that dune geometry responds to changes in flow on diurnal (tidal flux), synoptic (storm events) and seasonal (annual hydrograph) time scales, and that these responses display dominantly counterclockwise hysteretic behaviour (e.g. Pretious & Blench, 1951; Allen, 1973, 1974, 1982; Terwindt & Brouwer, 1986; Julien *et al.*, 2002; Villard & Church, 2003, 2005; Kostaschuk & Best, 2005) where changes in dune height and length lag the changes in flow. Height is observed to respond more directly to flow variability, while

length does not change as quickly (Allen, 1982). However, the absence of high-resolution 3D topography in natural variable flows has limited the assessment of the underlying dynamics and variability in bedform response to unsteady flows.

The goal of this paper is to advance current understanding of sedimentary processes in large, sand-bedded, fluvially dominated, tidal environments. This requires an understanding of bed topography and, in estuarine environments where dunes dominate the channel bed, dune response to flow variability. Here, the dynamics of bed geometry are examined at the diurnal scale in the fluvially dominated, tidally modulated Fraser River Estuary. Measurements of dune geometry based on multibeam echosounding are presented over the course of the falling and rising limbs of the largest diurnal tidal flux within the spring–neap tidal cycle during a period of high riverine discharge. Morphological changes through time are quantified to identify patterns in sediment deposition and erosion at the bed to address: (i) how do dune dimensions respond to tidal scale variable flow; and (ii) what sedimentary processes control low-angle dune morphology? The supporting data set constitutes the most comprehensive documentation of LAD characteristics so far achieved.

METHODS

Field study site

The Fraser River Estuary (Fig. 1) is located on the south-west coast of British Columbia, where the Fraser River enters the Strait of Georgia. The Fraser River has a drainage area of 234 000 km^2, with a mean annual discharge of 3410 m^3 sec^{-1} measured at the Mission gauge [Water Survey of Canada (WSC) Station 08MH024], located 85 river kilometres upstream of the river mouth at Sand Heads (from WSC data collected between 1969 and 1987, and reported in McLean *et al.*, 1999). Peak flow and sediment discharge occur in mid to late spring, following seasonal snowmelt, with the mean annual flood measuring 9790 m^3 sec^{-1} (McLean *et al.*, 1999). Historically, sediment discharge at the mouth of the Main Arm of the Fraser River averaged 17 million tonnes per year, *ca* 3 million tonnes of which was sandy bed material (McLean *et al.*, 1999), although in recent decades dredging for navigation in the Main Arm has significantly reduced the sand volume reaching Sand Heads.

The river bifurcates in the estuarine reach where the single inflowing channel splits into the North and Main Arms (Fig. 1). Further downstream the North Arm divides again, giving rise to the Middle Arm, and the Main Arm splits

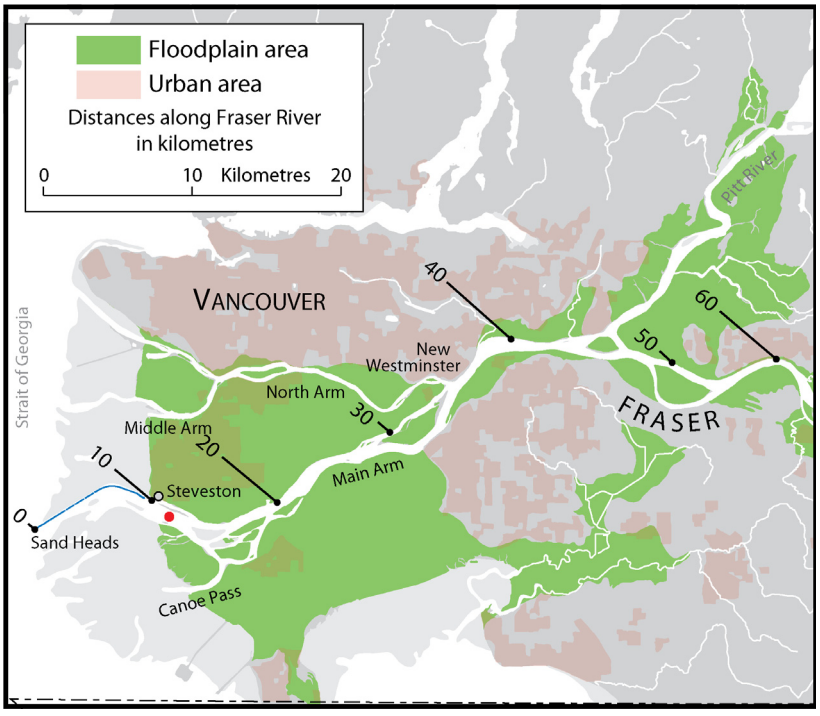

Fig. 1. Fraser River Estuary showing the field site (red dot).

to give rise to Canoe Pass. The Main Arm accommodates *ca* 70% of flow at peak annual river discharge (Western Canada Hydraulic Laboratories Ltd, 1977) and essentially the entire bed material load. The tidal pattern in the Fraser River Estuary is classified as mixed but mainly semi-diurnal, with a maximum tidal range of 5 m during spring tides (Kostaschuk *et al.*, 1989). During periods of low river discharge, a salt wedge enters the Main Arm (Kostaschuk & Luternauer, 1989), with an upstream limit reaching as far as New Westminster (*ca* 34 km upstream of the river mouth) (Dashtgard *et al.*, 2012) and Deas Island (*ca* 20 km upstream the river mouth) at mean annual discharge (Ages & Woollard, 1976). The study reach is located in the Main Arm of the Fraser River south of Steveston (Fig. 1). Data were collected along transects conducted over an area covering *ca* 1·0 km in the stream-wise direction and *ca* 0·5 km in the cross-stream direction (Fig. 2). Median bed material grain size (D_{50}) at the site was 0·27 mm during surveys for the present study (Bradley *et al.*, 2013), which is consistent with other work in the estuary showing that D_{50} in the estuary is 0·25 to 0·32 mm with little seasonal and spatial variation (Kostaschuk *et al.*, 1989; McLaren & Ren, 1995).

In the Main Arm of the Fraser River Estuary, dune heights are typically 1 to 2 m and lengths are 20 to 50 m, although dunes over 5 m high and 100 m long have been recorded (Pretious & Blench, 1951; Kostaschuk *et al.*, 1989). Kostaschuk *et al.* (1989) found that heights and lengths changed seasonally in response to fluctuations in river discharge. Dunes were relatively small in April and early May, reaching a maximum size in June, and then decreasing in size coincident with the decrease in sediment deposition through to September (see also Villard & Church, 2005). An annual channel dredging programme is typically conducted from August through to March, which results in planing of the channel bed (Villard & Church, 2005). On a shorter time scale, dune geometry in the Fraser River Estuary varies in response to tidal

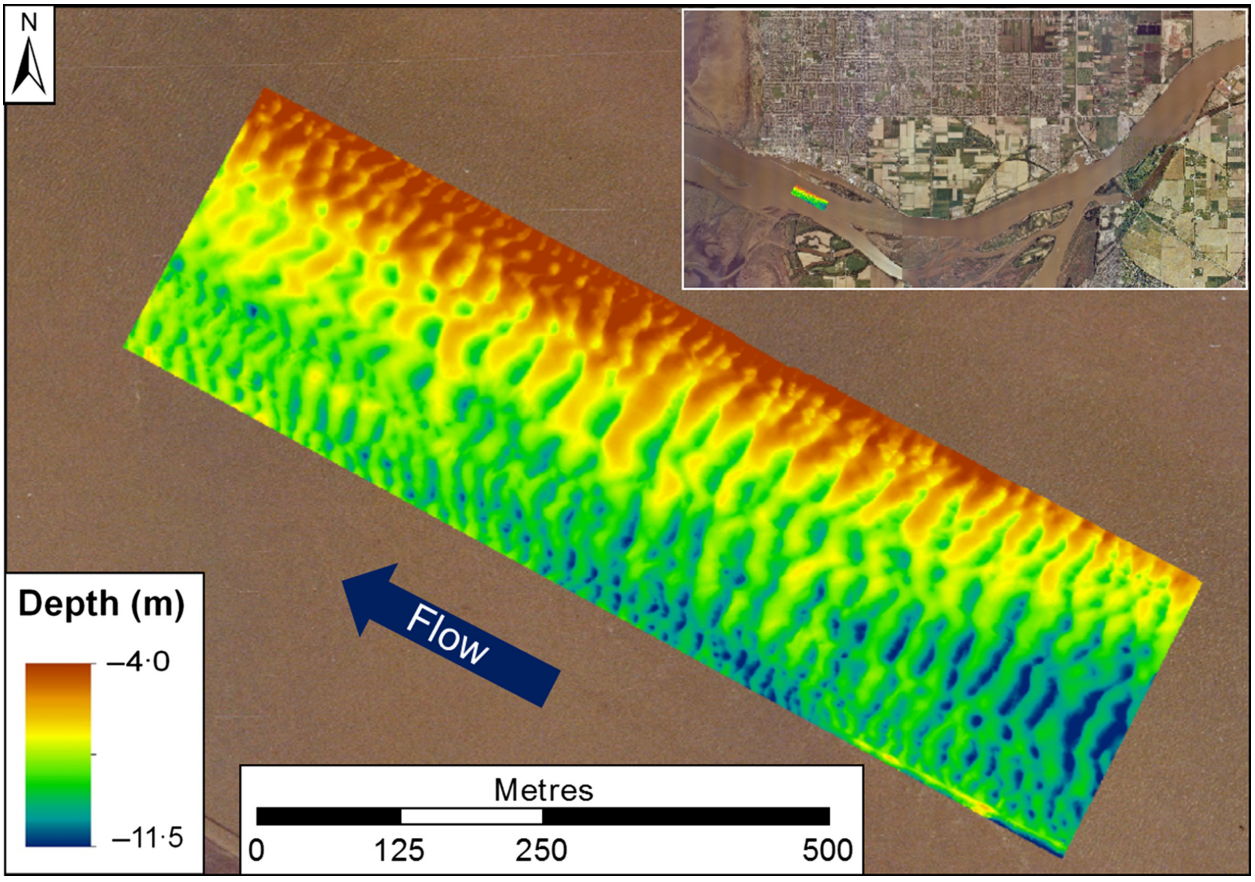

Fig. 2. Bathymetric map of the study site. The blue arrow indicates the direction of river flow. Inset shows the location of the study site within the Main Arm of the Fraser River.

flux (Kostaschuk *et al.*, 1989; Kostaschuk & Ilersich, 1995; Kostaschuk & Best, 2005).

Observations for the present study were made on 14 June 2010, coinciding with the largest spring tide of the lunar cycle and with elevated river discharge. Discharge is not recorded at Steveston, but a reasonable estimate of mean daily discharge can be obtained by using the recorded mean daily discharge from the nearest station on the river (Mission gauge). This yields a mean daily discharge of 6950 m^3 sec^{-1} for 14 June 2010 (Fig. 3A), which preceded the peak daily mean discharge on 28 June 2010 of 7490 m^3 sec^{-1}, one of the lowest annual peak flows on record. The only significant tributary below Mission, Pitt River, was ungauged in 2010, but probably contributed <100 m^3 sec^{-1} to the discharge at Mission. The actual discharge at Steveston will lag about one day from these data owing to the travel time from Mission to Steveston. Furthermore, tidal forcing strongly affects the actual discharge at Steveston because flooding tidal water slows, then accelerates river outflow. On 14 June 2010, the first high tide of the survey was +3·8 m, low tide was +0·40 m, and the second high tide was +4·3 m (Fig. 3B).

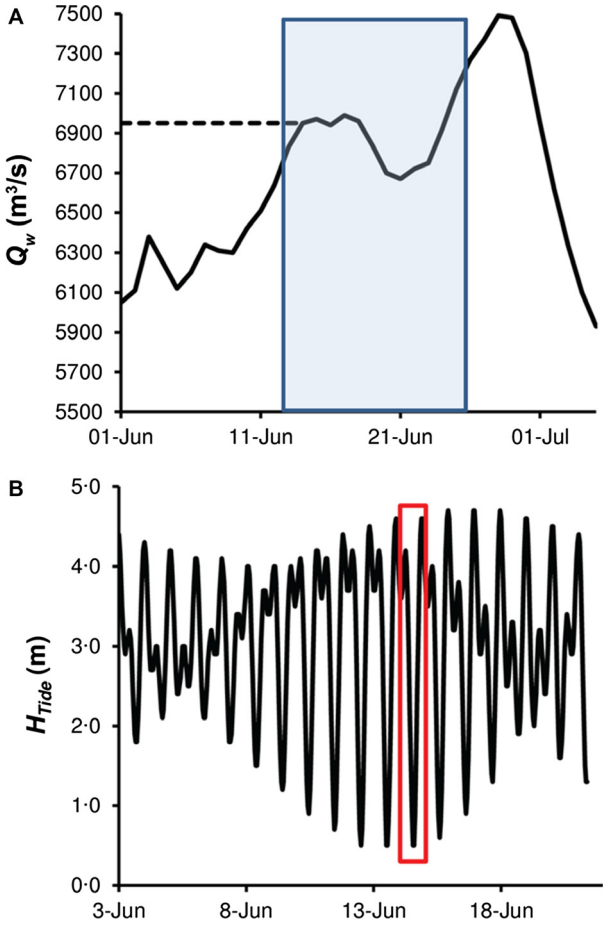

Fig. 3. (A) Hydrograph for mean daily discharge in Fraser River at Mission for June 2010. The dashed line indicates the mean daily discharge calculated for 14 June 2010. Discharge data from WSC station 08MH024 are available online at http://www.wsc.ec.gc.ca (accessed on 2 August 2012). (B) Water level recorded at Steveston Gauging Station (08MH028) of the neap–spring tidal cycle during which data were collected. Tidal height (H_{Tide}) is relative to geodetic datum. The red box indicates the diurnal tidal cycle over which data for this project were collected.

Data collection

Three-dimensional bathymetric data analysed in this paper come from a larger data set collected aboard the 7 m long *R/V Lake Itasca* between 12 and 17 June 2010, using a Reson 7101 Seabat® Multibeam Echosounder (MBES; Teledyne Reson A/S, Slangerup, Denmark). The MBES sonar head emits 511 equiangular beam soundings per ping to cover a swath area of 150° (*ca* 7·5X water depth) with a vertical resolution of *ca* 1·5 cm (Reson Inc., 2009). Spatial positioning of the MBES was accomplished using a Trimble Real Time Kinematic Global Positioning System (RTK GPS; Trimble Navigation Limited, Sunnyvale, CA, USA) with a static base station that sent corrections to the rover head at 1 Hz. Positional accuracy of the GPS unit when running in RTK survey mode is ±0·01 m horizontally and ±0·02 m vertically. Heading, pitch, heave and roll of the vessel were measured using an Applanix POS MV V3 gyroscope inertial guidance system (Applanix Corporation, Richmond Hill, ON, Canada). The system provides information to correct for the effects of horizontal and lateral vessel motion during survey operations.

This study focuses on eight surveys taken over the tidal cycle on 14 June 2010, chosen to correspond with the highest tidal fall of the cycle. Each survey is labelled according to its position on the tidal cycle as 'High Falling Tide' (HFT), 'Mid Falling Tide' (MFT), 'Low Falling Tide' (LFT), 'Low Tide' (LT), 'Low Rising Tide' (LRT), 'Mid Rising Tide' (MRT), 'High Rising Tide' (HRT) and 'High Tide' (HT) (Fig. 4). A salt wedge was observed in the channel around HT but did not result in the movement of sediment upstream.

A Teledyne RD Instruments 1200 kHz Rio Grande Workhorse® acoustic Doppler current

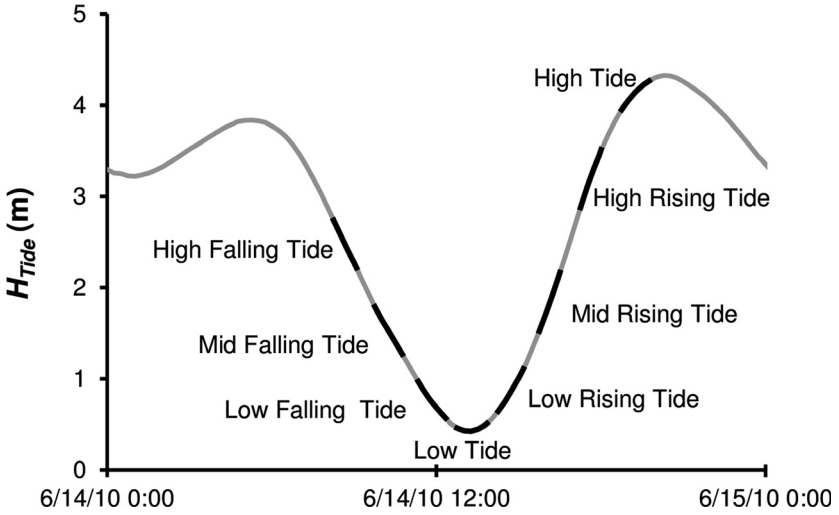

Fig. 4. Tidal cycle for 14 June 2010. Grey line shows the tidal stage (m) over which data were collected and the black lines are the individual surveys taken to characterize the fall and rise of the tide. Tidal height (H_{Tide}) is relative to geodetic datum.

profiler (ADCP; Teledyne Reson A/S) was also deployed from the *R/V Lake Itasca* and used to calculate mean velocities along the centre of the mapped study area (Fig. 2). The ADCP backscatter was calibrated against US Geological Survey P-63 point-integrated samples to provide depth-averaged sediment concentrations (<*SSC*>) (see Bradley *et al.* 2013 for additional detail on the calibration and analysis of these data). The position of the ADCP was recorded by a differential GPS (DGPS) system corrected by a Canadian Coast Guard beacon located *ca* 1·7 km south of the study site. Positional accuracy of the DGPS is 0·25 m horizontally and 0·50 m vertically.

Data processing

Raw MBES data were imported into CARIS HIPS® software (Caris, Fredericton, NB, Canada) for post processing to correct for changes in tidal stage, pitch, heave, roll and sound velocity, and to remove spurious data points. The data were then entered into ArcGIS® (Esri, Redlands, CA, USA) and gridded at 1 m spatial resolution for further analysis of channel bed characteristics for each of the eight surveys. A correlation analysis on the cross-stream depth data showed that topographic variability across the channel increased significantly at *ca* 30 m separation. To extract measurements of the bed from the topographic maps, 26 stream-wise transects, spaced at 10 m cross-channel intervals, were laid over the base maps. Points were extracted at 1 m intervals along each of these lines and tagged with the position (easting and northing) and depth of bed below the water surface.

Individual bed features were distinguished by identifying consecutive local minimum–maximum–minimum in the bed elevation along each bed transect. The length (L) of all features was measured as the distance from consecutive minimum to minimum. Features with a length below two standard deviations of the mean length for the transect were removed from the data set. This effectively filtered out features with lengths less than a few metres, which would have been distorted by the 1 m resolution of the maps. All other features were considered unique dunes. Height (H) of all remaining features in the data set was measured as the vertical distance measured from the crest (local maximum) to the trough (local minimum) of identified bedforms. Lee slope angle (θ_{Lee}) was measured as the steepest portion of the slope downstream of each crest following Kostaschuk (2006). Stoss slope angle (θ_{Stoss}) was measured from the upstream trough to the crest. Dune symmetry ratio (L_s/L) was calculated as the stoss side length (L_s) divided by the total dune length, such that a perfectly symmetrical dune has a ratio of 0·5. Successive topographic base maps were differenced to give the change in bed elevation between each survey, and to qualitatively display patterns of deposition and erosion on the channel bed.

The properties of individual bedform measurements along each transect are treated as a sample of the spatial variability in individual, laterally continuous bedforms. Spatially averaged bedform properties were calculated along with the standard error of the mean using all samples of bedform properties in the mapped area. Another approach would be to have aver-

aged across each laterally continuous bedform crest, and then averaged the bedform properties for each laterally continuous bedform. However, the bedform crestlines are highly bifurcated, so identifying which crestline to average along would be arbitrary. Whether mean bedform properties are created for each laterally continuous bedform, then averaged, or for the whole bedform field, does not make a substantial difference in the values. Therefore, the simpler spatial averages of the whole bedform field and associated standard errors are reported.

Frequency polygons were constructed from the spatially variable bedform properties in the mapped area to compare the distributions of dune heights, lengths, aspect ratios and lee slope angles for each of the surveys. This was achieved by dividing each data set into equal-sized bins ranging from the lowest to highest values. Bins for dune height, length, aspect ratio and lee slope angle were set at 0·1 m, 1 m, 0·005 and 5°, respectively.

OBSERVATIONS

Bed topography

Bathymetric maps generated from the MBES data show a trend of decreasing elevation across the channel, with a lateral bar on the north (right bank) side creating an area of higher elevation, and scour on the south side where a secondary channel re-enters the Main Arm downstream of a series of islands (Fig. 2). The bed surface is covered in dunes, with the largest dunes occurring along the centre of the channel. There were no superimposed secondary features. These large dunes display near-symmetrical cross-sectional morphology, with a mean slope symmetry ratio (L_S/L) of 0·59, and range of 0·10 to 0·93.

Dune heights, lengths and aspect ratios

The overall distribution of dune heights and lengths appears to be stable over the observed tidal cycle (Fig. 5). Maps of height distributions for five surveys over the tidal cycle (Fig. 5A) show that the highest dunes are consistently located in the centre of the study area, and in the upstream three-quarters of the length of the site. Maps of length distribution for the same five surveys (Fig. 5B) show the longest dunes occurring in the centre of the study area, with the dunes of maximum length corresponding to the area of the dunes with the greatest heights. Mean dune height for the entire bed, calculated over all surveys, is 1·16 m, mean dune length is 25 m and mean aspect ratio is 0·046.

Figure 6 shows the variation in the mean and standard error of dune height, length and aspect ratio over the tidal cycle. Overlap of error bars suggests that caution should be exercised when interpreting the changes between certain survey times. The pattern of change for dune height is highly coherent with mean velocity and suspended sediment concentration. No substantial change in mean dune height occurred between HFT and MFT (Fig. 6A; Table 1) when river discharge was slowly increasing as the tide ebbed: HFT and MFT correspond to low $\langle SSC \rangle$ and $\langle u \rangle$, but both were beginning to increase. At LFT, the highest $\langle SSC \rangle$ in the water column occurred and $\langle u \rangle$ continued to increase until it reached a peak at LT. Dune height increased at LT, while $\langle SSC \rangle$ dropped slightly from the previous survey. A substantial increase in H occurred for each survey from LT to MRT and remained constant through to HRT. Suspended sediment concentration dropped over this time period, and velocity slowed as the tidal influx imposed increasing opposition to river flow. At HT, H decreased while $\langle u \rangle$ fell to its lowest recorded value, as did $\langle SSC \rangle$. Over the course of the tidal cycle, maximum dune heights increased while minimum dune heights increased substantially at HRT, followed by a return to a minimum value similar to previous survey times (Table 1).

Dune L shows a pattern of cyclical variability (Fig. 6B; Table 1) similar to that of H, but with an anomalous measurement at LT and much reduced relative range of variation. The difference in L from the beginning of the tidal cycle to the end was a modest 1 m increase (<5%) which is the same as the grid spacing of the maps, suggesting there may have been no substantive variation at all. Similarly, both maximum and minimum lengths measured over the tidal cycle show a net increase from HFT to HT. The combination of overall increase of H and L, and the lagged cyclic response of H to flow variability results in a pattern of H/L over the tidal cycle that is more variable than H alone (Fig. 6C; Table 1). Aspect ratio (H/L) fluctuated between 0·044 and 0·046 between HFT and LT, but then increased to the maximum observed mean value of 0·049 at LRT as the tidal height began to rise, followed by a decrease towards HT.

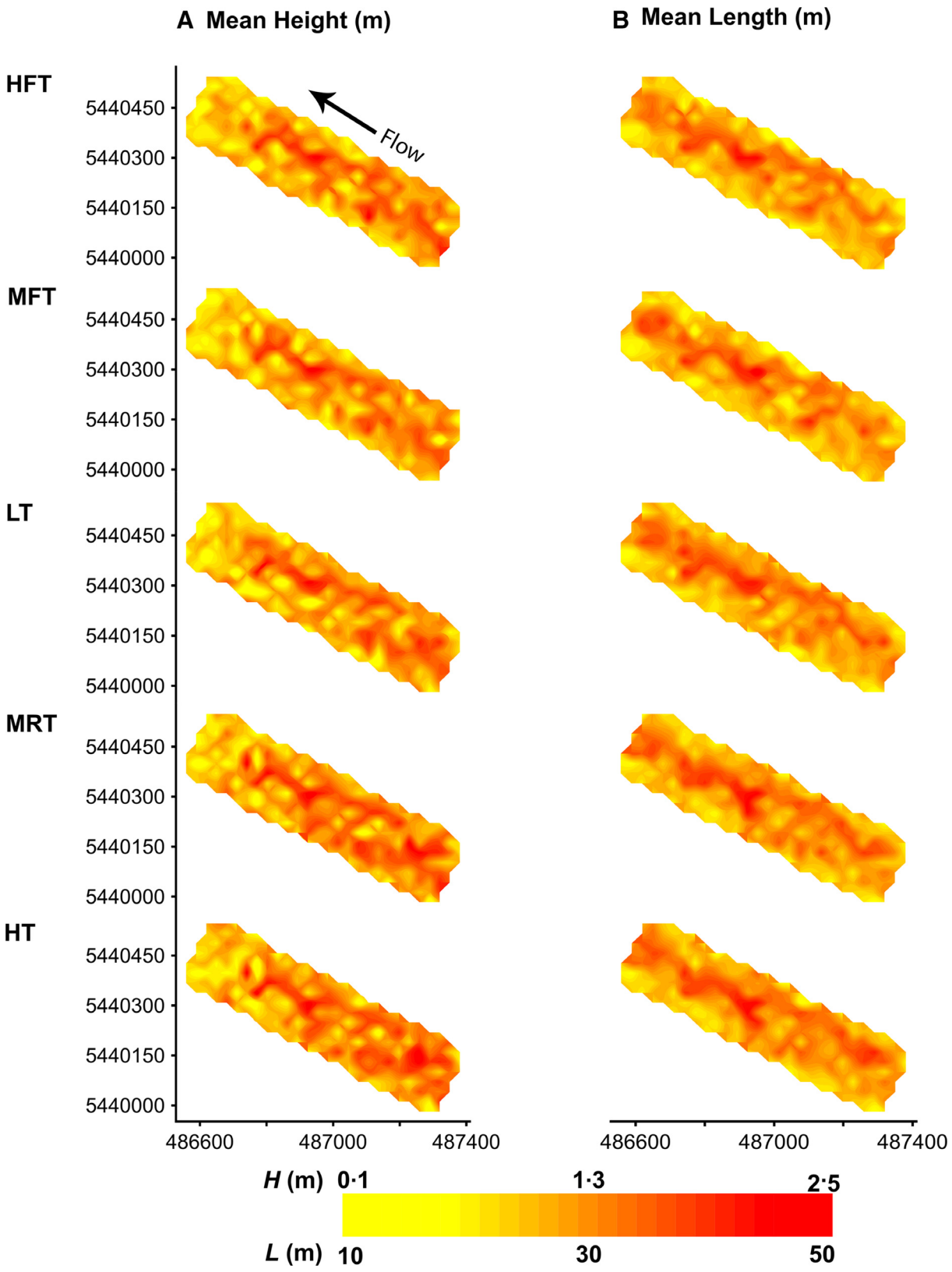

Fig. 5. Selected spatial variability maps for dune height (left) and dune length (right) during the 14 June 2010 tidal cycle. Horizontal and vertical axes are 'easting' and 'northing'. HFT, High Falling Tide; MFT, Mid Falling Tide; LT, Low Tide; MRT, Mid Rising Tide; and HT, High Tide.

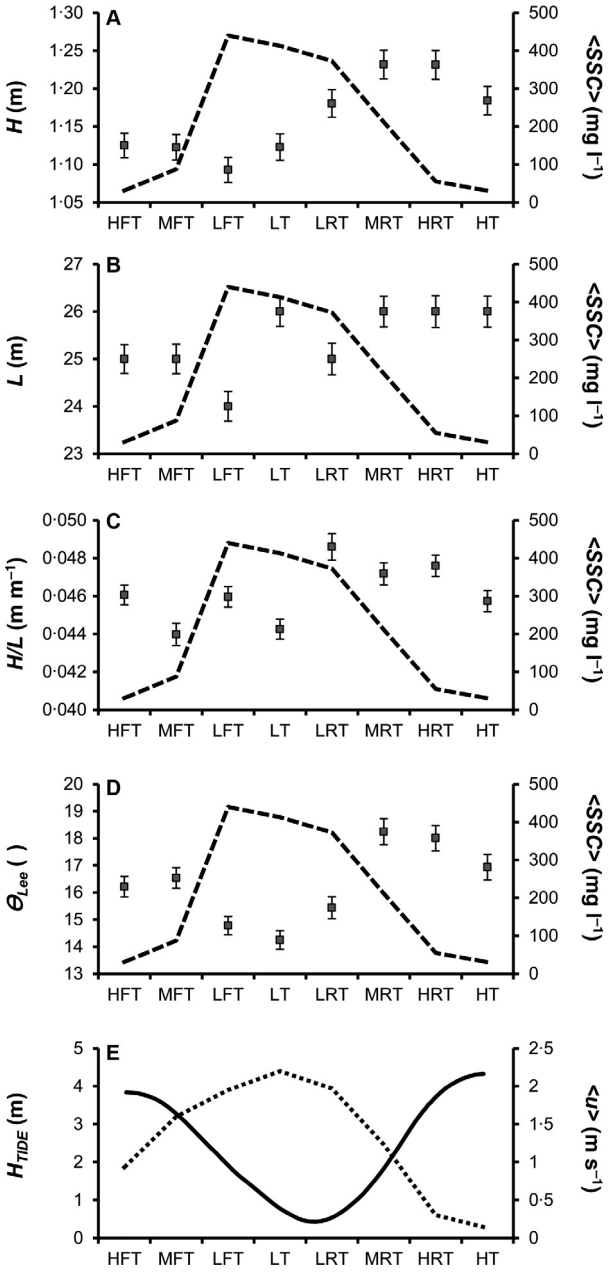

Fig. 6. Mean dune: (A) height; (B) length; (C) aspect ratio; (D) lee slope angle; and (E) depth-averaged velocity (dashed line) and tidal height relative to geodetic datum (solid line). The dashed line in (A) to (D) denotes suspended sediment concentration. Error bars denote standard error of the mean.

Frequency polygons for *H*, *L* and *H/L* (Fig. 7) show that the distribution of each geometric property retained the same general pattern over the tidal cycle. The distributions for height and length (Fig. 7A and B) are unimodal with positive skew, while the distributions for aspect ratio (Fig. 7C) are closer to being normally distributed, with fluctuating skewness and negative values at MFT, MRT and HT. Comparison of the distributions using an equal variance Student's *t*-test generally supports the current visual interpretations of changes in the mean properties. The distributions of *L* are all statistically the same at the 95% confidence interval. Distributons of *H* and θ_{Lee} are statistically the same for adjacent portions of the tide cycle where the error bars overlap, statistically different where the change exceeds the error bars, and statistically the same at the beginning and end of the tide cycle. Distributions of *H/L* inherit variability from *H* and *L* and show no statistically significant patterns.

Lee slope angles

Maps of the distribution of θ_{Lee} for five select surveys over the tidal cycle (Fig. 8) show that dune lee angles were highest in the upstream two-thirds of the study area at all tidal stages. Lee angle decreased from HFT to LT, followed by an increase from LT to HT. Measured θ_{Lee} for the entire bed over the tidal cycle is 16·3°, indicating that the dunes in the study area were predominantly LADs. However, Fig. 7D reveals that, at all stages of the tide cycle, a small proportion of the dunes are HADs. The highest measured angle is 44·1° and the lowest is 0·5°. The steepest angles were in the upper three-quarters of the study site, and the changes in θ_{Lee} are most pronounced in this region (Fig. 8). The pattern of change in mean θ_{Lee} is similar to that of *H* and coincides with patterns of <*u*> and <*SSC*> (Fig. 6D). Extreme angles follow a pattern similar to that of θ_{Lee} but maximum and minimum angles, respectively, show larger and lesser fluctuations (Table 1). The frequency distribution for θ_{Lee} (Fig. 7D) has a unimodal pattern with positive skewness that remains relatively stable over the survey period. Skewness values decrease from HFT to MRT, and then increase towards HT. The frequency of θ_{Lee} >30°, the putative threshold between high and low-angle dunes, increases from *ca* 5% at LT to nearly 25% at HT.

Relations between height (*H*), length (*L*), aspect ratio (*H/L*) and lee slope angle θ_{Lee}

There is tremendous scatter in relations between the geometric properties of individual dunes (Fig. 9A to C), so relations between mean values for each tidal stage were explored using correlation analysis (Fig. 9E to H). The non-parametric Spearman Rank correlation test (Bradley, 1968)

Table 1. Mean, maximum and minimum geometric properties of the dunes for each survey time in the study period. HFT, High Falling Tide; MFT, Mid Falling Tide; LFT, Low Falling Tide; LT, Low Tide; LRT, Low Rising Tide; MRT, Mid Rising Tide; HRT, High Rising Tide; and HT, High Tide.

	Height (m)					Length (m)				
Position in tidal cycle	Mean	Max	Min	SD	CV %	Mean	Max	Min	SD	CV %
HFT	1·12	2·67	0·054	0·50	0·44	25	62	3	9	0·37
MFT	1·12	2·62	0·040	0·52	0·46	25	64	5	9	0·38
LFT	1·09	2·82	0·072	0·51	0·47	24	64	5	10	0·39
LT	1·12	2·83	0·059	0·53	0·47	26	56	4	9	0·37
LRT	1·18	2·65	0·025	0·54	0·46	25	57	5	10	0·39
MRT	1·21	2·67	0·033	0·57	0·47	26	58	6	10	0·38
HRT	1·23	2·69	0·073	0·57	0·46	26	60	6	10	0·38
HT	1·18	2·73	0·059	0·56	0·47	26	56	6	10	0·37

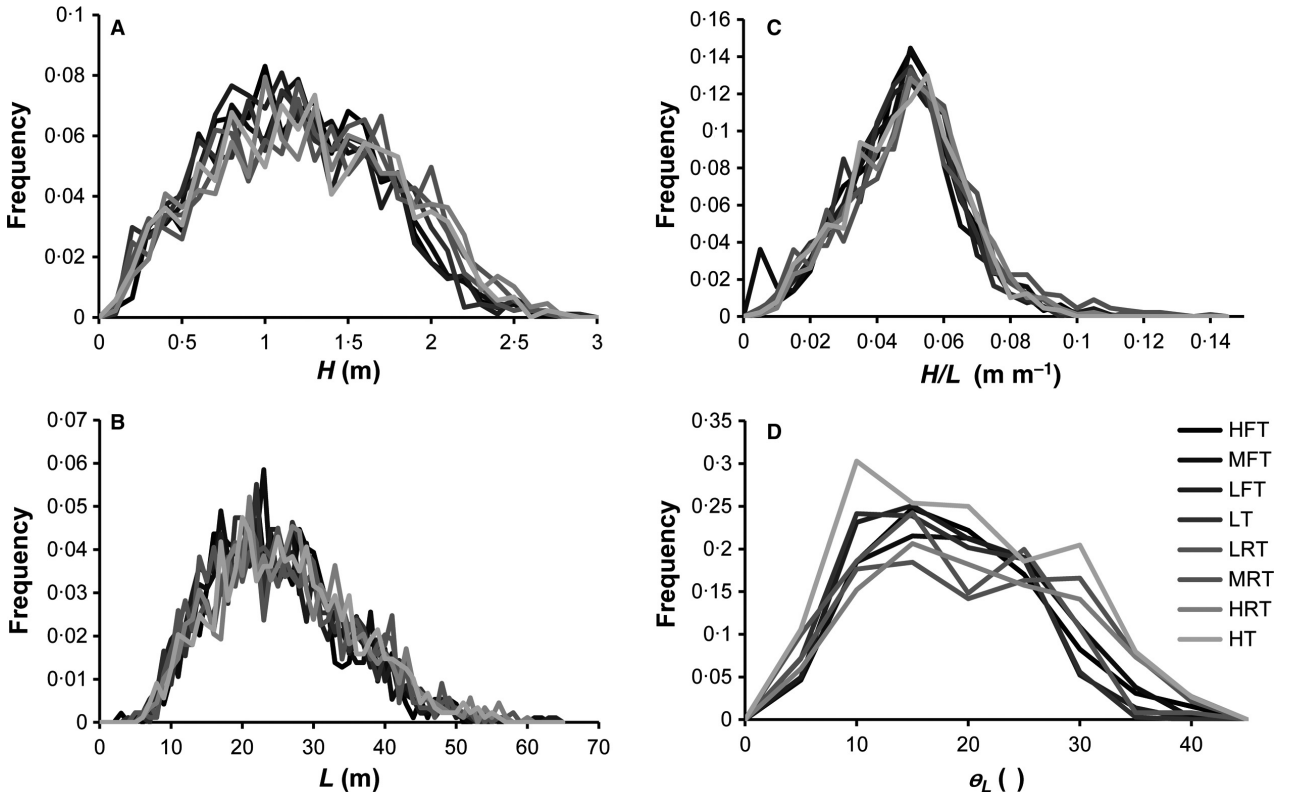

Fig. 7. Frequency polygons showing the distributions of dune: (A) height (0·1 m bins); (B) length (5 m bins); (C) aspect ratio (0·005 bins); and (D) lee slope angle (5° bins) over the tidal cycle.

was chosen because it can be applied without constraints posed by the underlying distribution of the variables. Statistical significance is assessed using the Student's *t*-test.

There are statistically significant relations between θ_{Lee} and *H,* as well as *H* and *L* at the 95% confidence level. There is no statistically significant relation between θ_{Lee} and *L*. There is also a statistically significant relation between θ_{Lee} and *H*/*L* at the 90% confidence interval, but this probably reflects the strong correlation between θ_{Lee} and *H*. The weakness of the correlations is at least

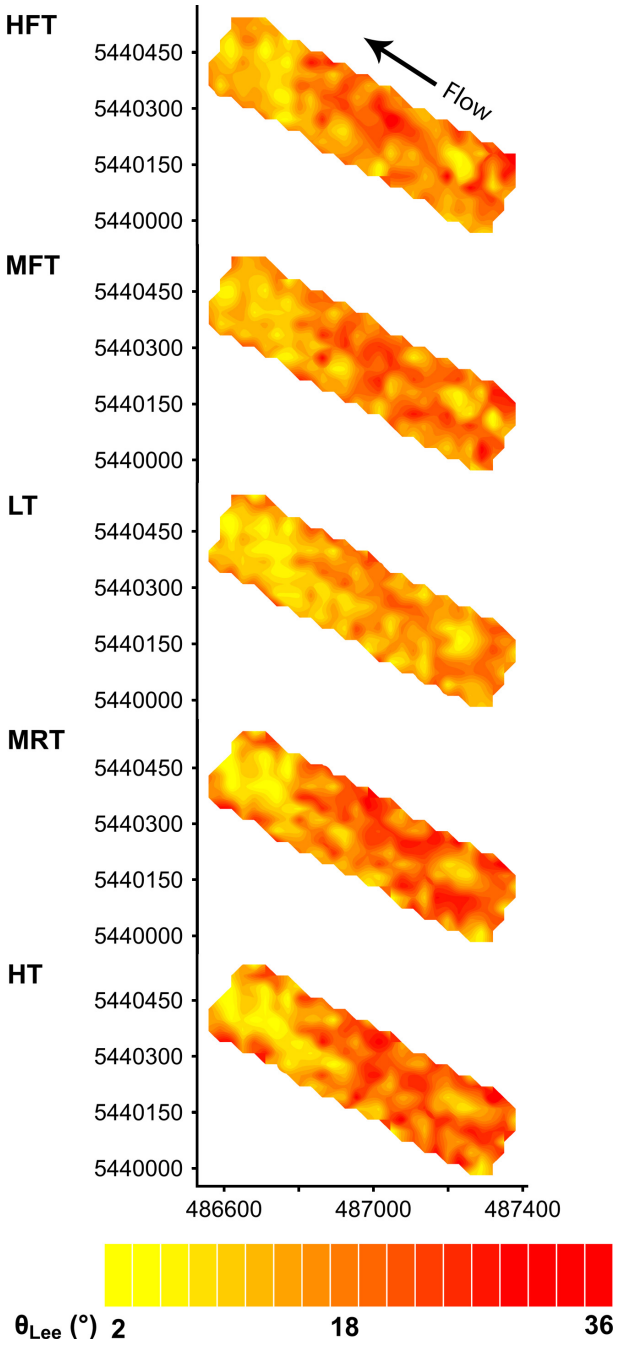

Fig. 8. Selected spatial variability maps for distribution of lee slope angles (θ_{Lee}) during the 14 June 2010 tidal cycle. Horizontal and vertical axes are 'easting' and 'northing'. HFT, High Falling Tide; MFT, Mid Falling Tide; LT, Low Tide; MRT, Mid Rising Tide; and HT, High Tide.

partially due to hysteretic relations, or lag, between the variables. There is a closed hysteresis loop between θ_{Lee} and *H,* as well as open loops between θ_{Lee} and *L* and *H* and *L*, the latter suggesting that the dunes are growing. The strength of the correlation between θ_{Lee} and *H* and the closed hysteresis loop suggest that the adjustments in lee angle and dune height are related.

Erosion and deposition patterns in the dune field

The changes in bedform geometry are associated with patterns of erosion and deposition of sand in the dune field. The change in bed topography between HFT and MFT (Fig. 10A) is minimal relative to the other time sequences, with isolated patches of deposition and erosion mostly occurring on the lower lee slope and patches of erosion on the south side of the channel. The difference in topography between MFT and LFT (Fig. 10B) is more pronounced, with erosion predominantly on the stoss slope, along the crest and along the uppermost lee of the dunes, and deposition on the lowermost lee and downstream trough. This pattern, coincident with increasing flow velocity, results in a decrease in dune height and lee angle.

From LFT to LT (Fig. 10C), the depositional zone in the trough expands and extends further up the lee slope, and erosion continues over the stoss slope, along the crestline and the upper lee slope. This pattern does not result in significant changes in either mean height or lee angle, however. Between LT and LRT, erosion is limited in the uppermost lee area and crest but continues on the stoss slope, while deposition is still occurring in the trough and increasingly up the lee slope, almost to the crest in some locations. An increase in height and lee angle is observed over this time, due to deposition of sediment higher up on the lee slope.

The change in topography between LRT and MRT (Fig. 10D) is much less compared to previous surveys because mean velocity and suspended sediment concentration decline in response to the rising tide. There is deposition on the crest and upper stoss in some areas, resulting in an increase in height and lee angle. From MRT to HT (Fig. 10E) there is sporadic erosion and deposition in troughs and on lee slopes but mean height, length and lee slope angle values do not change significantly, reflecting the weak velocity and sediment movement on the approach to high tide.

DISCUSSION

The majority of the dunes observed in this study have lee sides considerably less than 30° and

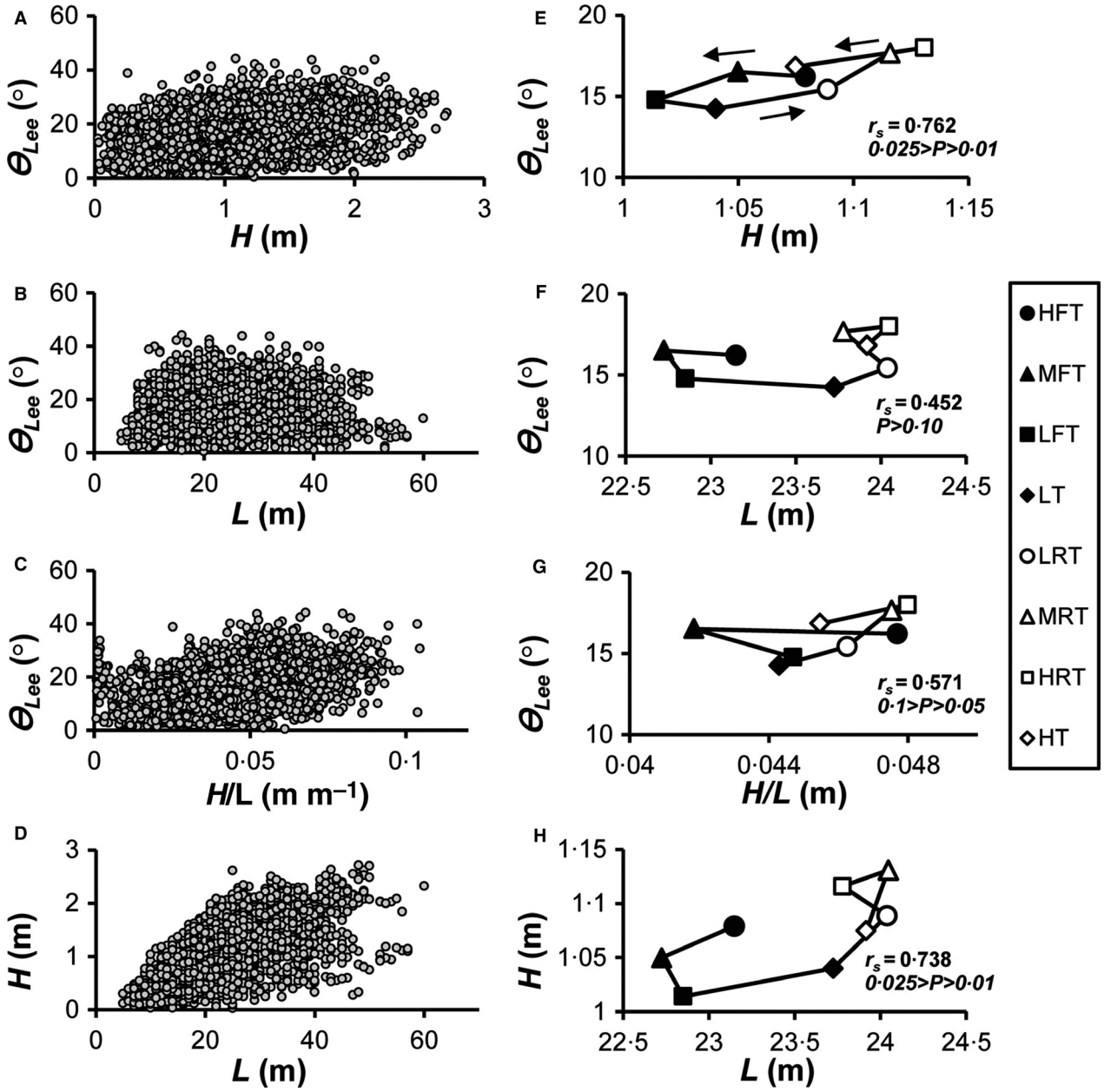

Fig. 9. Relations between dune lee angle (θ_{Lee}), height (H), length (L) and aspect ratio (H/L). (A) to (D) show individual dunes at each tidal stage and (D) to (H) show the mean value at each stage. Correlation coefficients (r_s) were calculated using Rank Spearman Correlation. The P-value calculated from a t-distribution is inaccurate when there are less than 11 observations, so the P-value is determined from a t-statistics table and reported as ranges of values. The arrows in (E) highlight an obviously complete hysteresis loop between H and θ_{Lee}. HFT, High Falling Tide; MFT, Mid Falling Tide; LFT, Low Falling Tide; LT, Low Tide; LRT, Low Rising Tide; MRT, Mid Rising Tide; HRT, High Rising Tide; and HT, High Tide.

are classified as low-angle dunes (LADs), which is consistent with previous observations in Fraser River Estuary (Kostaschuk & Villard, 1996, 1999; Kostaschuk & Best, 2005; Bradley *et al.*, 2013), and in other estuaries and large rivers (e.g. Smith & McLean, 1977; Soulsby *et al.*, 1991; Parsons *et al.*, 2005; Kostaschuk, 2006; Kostaschuk *et al.*, 2009). The detailed Multibeam Echosounder (MBES) observations in the present study enable two critical issues regarding LADs to be addressed; (i) the response of dune morphology to highly unsteady flow; and (ii) the sedimentary processes responsible for low-angle dune lees.

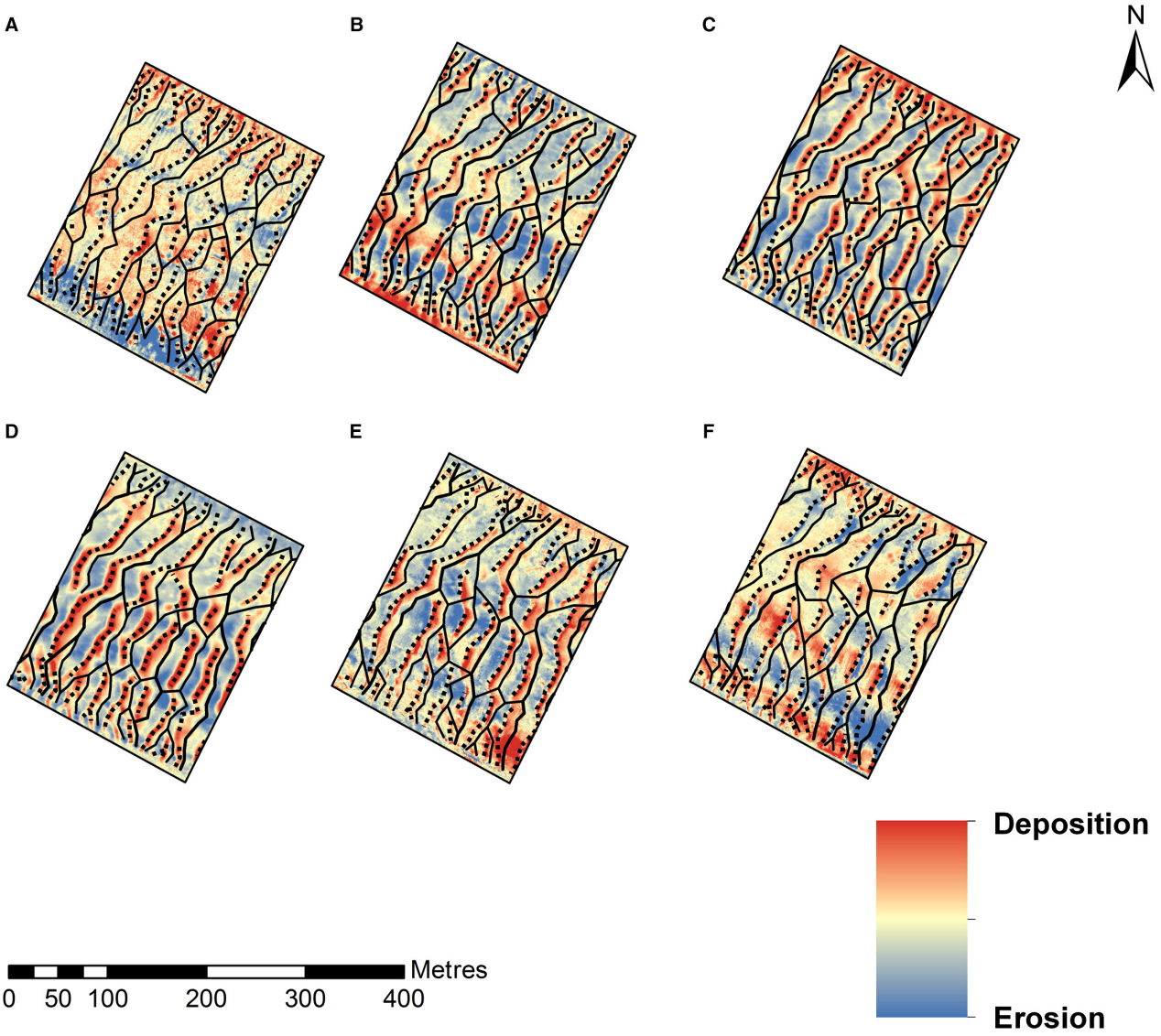

Fig. 10. Difference maps between surveys over the tidal cycle. (A) HFT to MFT, (B) MFT to LFT, (C) LFT to LT, (D) LT to LRT, (E) LRT to MRT and (F) MRT to HT. Solid lines indicate crestlines while dotted lines are the trough lines at the end of the time period of individual difference maps. Central part of study area only displayed. The through-going longitudinal stripes may be evidence of preferred 'alleys' of sand transport, but may equally be evidence of imperfect matching of the water surface (the reference plane) between successive survey track lines. HFT, High Falling Tide; MFT, Mid Falling Tide; LFT, Low Falling Tide; LT, Low Tide; LRT, Low Rising Tide; MRT, Mid Rising Tide; HRT, High Rising Tide; and HT, High Tide.

How do dune dimensions respond to tidal scale variable flow?

There is often a lag between flow and dune size on a variety of time scales: the diurnal tidal scale (e.g. Kostaschuk & Best, 2005); the bi-monthly neap–spring lunar scale (e.g. Allen, 1969; Allen & Friend, 1976; Terwindt & Brouwer, 1986; Davis & Flemming, 1991; Rhodes, 1992) and the seasonal freshet scale (e.g. Pretious & Blench, 1951; Villard & Church, 2005). Allen (1976; see later summary in Allen, 1982) argued that dune height responds to flow variability more quickly than dune length because it is necessary for a larger amount of sediment to be moved to change the dune length than the height. Allen (1976) used a simple numerical model to predict how dunes changed with flow by assuming that while dune height adjusted with the flow, length remained constant for the lifespan of a dune but new dunes emerged at a wavelength scaled to the flow as it

changed. These simple assumptions reproduced the lag between dune height and length with flow. More recent work has suggested that wider, more rounded hysteretic loops indicate a greater lag time than tighter, more rectilinear ones (Dalrymple & Rhodes, 1995) and this has been confirmed in a number of empirical studies (Kostaschuk *et al.*, 1989; Gabel, 1993; Kostaschuk & Ilersich, 1995; Julien *et al.*, 2002; Wilbers & ten Brinke, 2003; Wilbers, 2004; Kostaschuk & Best, 2005).

The present results show that dune height does respond more rapidly to the change in flow than dune length, which changes little over the course of the tidal cycle, as highlighted by Allen (1976). The observed changes in height and lee slope angle are associated with erosion and deposition patterns over the dunes as flow velocity and sediment suspension change. As the tide falls and flow velocity increases in the channel, there is erosion of the stoss slope and eventually the dune crests as the stage approaches low tide. This is coincident with deposition in the dune troughs, causing a decline in the dune lee slope. The increase in suspended sediment concentration suggests that this transfer from the stoss and crest to the dune trough occurs via sediment bypassing the lee slope. As the tide rises, the sediment moves as bedload and accumulates on the dune stoss and lee slope, increasing the dune height and steepening the lee slope.

Mean H, L, H/L, θ_{Lee} and $\langle SSC \rangle$ all show counterclockwise hysteresis with flow velocity (Fig. 11), indicating that the response of the mean geometry lags diurnal scale flow fluctuations. Kostaschuk & Best (2005) show clockwise hysteretic loops for height and aspect ratio. The fact that height adjusts more directly to changes in velocity could allow for greater variability in response (Dalrymple & Rhodes, 1995) which might explain the height result of Kostaschuk & Best (2005), although it is equally possible that these data reflect sampling bias. The data were collected by taking multiple surveys of a single transect line in the middle of the channel. Data collected along a single transect line would require a very high degree of locational precision to be strictly comparable and, as dune height has been shown to be highly variable along the crestline of a dune (Allen, 1982; Parsons *et al.*, 2005; Venditti *et al.*, 2005), any deviation from the original transect could introduce false variability.

What sedimentary processes control low-angle dune morphology?

The pre-eminent hypothesis for LAD morphology is deposition of suspended bed material in the trough and on the dune lee side, which acts to reduce dune height and lower the lee slope angle (see Kostaschuk *et al.*, 2009, for a recent review). This hypothesis is supported by numerical modelling (Johns *et al.*, 1990) that shows high flow velocities plane the dune crest and suspend sand that is deposited in the trough. Field observations have also suggested that increased sand transport in suspension, relative to bedload, is associated with flatter dunes and lower lee slope angles (Smith & McLean, 1977; Kostaschuk & Villard, 1996; Amsler & Schreider, 1999; Kostaschuk, 2000; Kostaschuk *et al.*, 2009). However, direct measurements of changes in dune lee angle with changes in suspended sediment flux have not been reported previously.

The present results support the hypothesis that LAD morphology is linked directly to sediment suspension. As flow accelerates in the channel and sediment goes into suspension, the lee angles decline (Fig. 6), confirming earlier speculation that sediment bypassing the crest and deposited in the bedform lee maintains LAD morphology (Kostaschuk, 2006; Kostaschuk *et al.*, 2009). In addition, lee angle varies directly with dune height (Fig. 9) and the complete hysteresis loop formed between θ_{Lee} and H suggests that the increase in sediment suspension is linked to a planing off of the crest of the dune. This is highlighted in the patterns of erosion and deposition between surveys (Fig. 10) which show that, as the flow accelerates, broad areas of the dune stoss slope and crest become erosional and the troughs become depositional.

While deposition from suspension clearly plays an important role in maintaining LAD morphology, it cannot be the sole determinant of low lee angles. Bedload transport rates also increase with flow and suspended flux rates, and should lead to deposition on the lee crest and avalanching into the dune trough which would steepen the lee angles. Low-angle dune morphology has been observed in large, coarse-grained, bedload-dominated rivers where little bed material is transported in suspension (Carling *et al.*, 2000a,b). The present authors suspect that the dynamics of sand flows generated by avalanching on the lee side may also be a significant factor. Over small-scale, high-angle dunes, a wedge of sand accumulates at the top

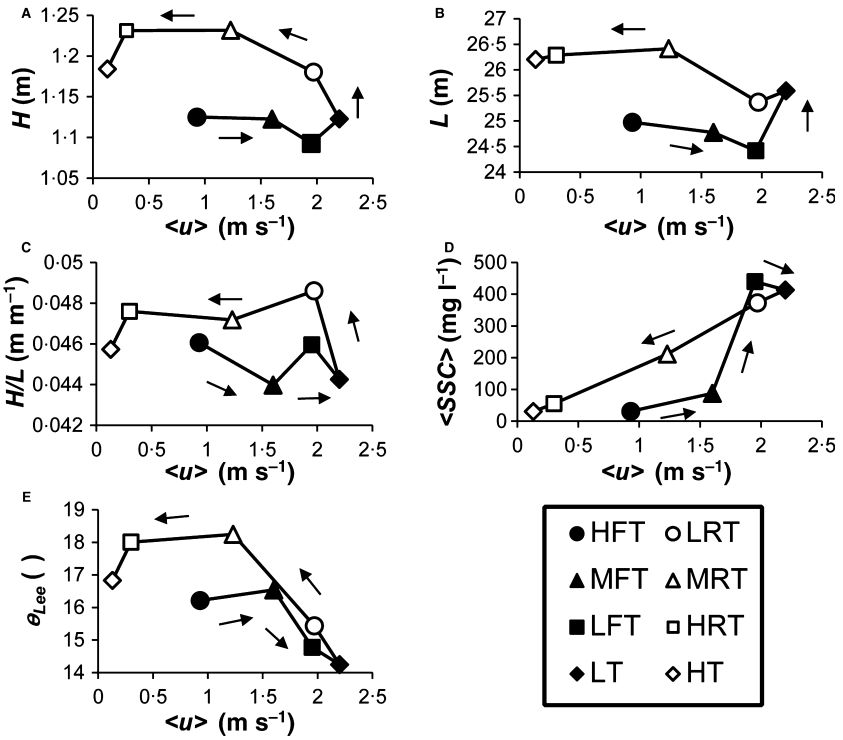

Fig. 11. Relation between mean velocity (<*u*>) and: (A) dune height (*H*); (B) dune length (*L*); (C) aspect ratio (*H/L*); (D) suspended sediment concentration (<*SSC*>); and (E) lee slope angle (θ_{Lee}). Arrows indicate direction of loop. HFT, High Falling Tide; MFT, Mid Falling Tide; LFT, Low Falling Tide; LT, Low Tide; LRT, Low Rising Tide; MRT, Mid Rising Tide; HRT, High Rising Tide; and HT, High Tide.

of the lee side and fails to form thin sand flows that come to rest at the static angle of repose (e.g. Allen, 1985; Hunter & Kocurek, 1986; Kleinhans, 2004). It has been shown that granular materials change volume when sheared (e.g. Reynolds, 1886; Bagnold, 1954) which causes dilation and increased excess pore water pressures in granular materials moving in water (Pailha & Pouliquen, 2009). It has also been shown that excess pore pressure in sand flows increases linearly with sand flow thickness, and that flows with higher pore pressures can move on much lower slopes than the static angle of repose (Pailha *et al.*, 2008; Pailha & Pouliquen, 2009). Assuming that the wedge of sand formed at the top of HADs also forms over LADs due to bedload and suspension deposition, and that its failure produces proportionally thicker flows than over small-scale, HADs, sand flow liquefaction could play a role in LAD development. Indeed, it is likely that the loosely structured deposits formed by suspension deposition on the dune brink point and the lee slope would be more likely to dilate upon mass failure, explaining why LADs are more common under suspension dominated conditions, especially when the trough is also filling with sediment bypassing the dune crest as has been shown here. It is not possible to unequivocally isolate topographic signatures of liquefied sand flow deposits from the current bathymetry. However, the possible role liquefied sand flows might play in forming low lee angles under high bedload and suspended bed material transport conditions needs to be examined critically.

CONCLUSIONS

The geometry and morphology of dunes in variable flows were examined in the tidally influenced, fluvially dominated flow in Fraser River Estuary, British Columbia, Canada. A patch of a dune field 1·0 km long and 0·5 km wide was mapped with a Multibeam Echosounder (MBES) over a diurnal tidal cycle. The dunes exhibited the low-angle morphology commonly observed in large sand-bedded river channels and estuaries. As the ocean tide fell, flow velocity and suspended sediment concentrations increased, then declined as the ocean tide rose causing the following changes in the dune field:

1 Dunes adjusted by relaxing the lee angle slope and flattening as the tide fell and flow increased, and more sediment was moved into suspension, bypassing the dune crest and depositing in the dune trough.

2 Dune height and lee angle have a counterclockwise hysteretic response to mean flow veloc-

ity, suggesting that changes in the bedform geometry lag changes in the flow, as has been observed in previous work in tidal environments.

3 Dune height forms a complete hysteresis loop with lee angle slope, suggesting that the relaxation of the lee slope is associated with the planing off of the dune crest.

4 The patterns of deposition and erosion over the tidal cycle support the observed changes in height and lee slope angle. As the tide falls, the dune stoss and crest are planed off and that material is deposited in the trough from suspension. As the tide rises, height and lee slope angle increase significantly due to persistent deposition on the crest and erosion in the trough.

The results highlight the complex response of dunes formed in variable flow and underline the need for further high-resolution observations of dune dynamics in unsteady flows under diurnal (tidal flux), synoptic (storm events) and seasonal (annual hydrograph) fluid forcing.

ACKNOWLEDGMENTS

This work was supported by the National Sciences and Engineering Research Council of Canada (NSERC) Discovery Grants to JGV, MC and RAK. MH was supported by a SFU Graduate Fellowship and the Department of Geography. RWB was supported by a NSERC Alexander Graham Bell Canada Graduate Scholarship. Steveston Gauging Station (08MH028) data were provided by Lynne Campo, Water Survey of Canada. Technical support and field assistance were kindly provided by Dan Duncan (UT), Maureen Attard (SFU) and Sally Haggerstone (SFU).

REFERENCES

Ages, A. and **Woollard, A**. (1976) The tides in the Fraser River Estuary. Pacific Marine Science Report 76-5. Institute of Ocean Sciences, Victoria, BC.

Allen, J.R.L. (1968) *Current Ripples: Their Relation to Patterns of Water and Sediment Motion*. Elsevier, New York, NY.

Allen, J.R.L. (1969) On the geometry of current ripples in relation to stability of fluid flow. *Geogr. Ann.*, **51**, 61–96.

Allen, J.R.L. (1973) Phase differences between bed configuration and flow in natural environments, and their geological relevance. *Sedimentology*, **20**, 323–329.

Allen, J.R.L. (1974) Reaction, relaxation and lag in natural sedimentary systems: general principles, examples and lessons. *Earth-Sci. Rev.*, **10**, 263–342.

Allen, J.R.L. (1976) Computational models for dune time-lag: general ideas, difficulties, and early results. *Sed. Geol.*, **15**, 1–53.

Allen, J.R.L. (1982) *Sedimentary Structures: Their Character and Physical Basis*, volumes 1 and 2. Elsevier, Amsterdam, 593 pp.

Allen, J.R.L. (1985) *Principles of Physical Sedimentology*. George Allen & Unwin, London.

Allen, J.R.L. and **Friend, P.F.** (1976) Changes in intertidal dunes during two spring-neap cycles, Lifeboat Station Bank, Wells-Next-The-Sea, Norfolk. *Sedimentology*, **23**, 329–346.

Amsler, M.L. and **Schreider, M.I**. (1999) Dune height prediction at floods in the Paraná River, Argentina. In: *River Sedimentation: Theory and Applications* (Eds A.W. Jayewardena, J.H.W. Lee and Y. Wang), pp. 615–620. A.A. Balkema, Brookfield, VT.

Ashley, G.M. (1990) Classification of large-scale subaqueous bedforms: a new look at an old problem. *J. Sed. Petrol.*, **60**, 160–172.

Bagnold, R.A. (1954) Experiments on a gravity-free dispersion of large solid spheres in a Newtonian fluid under shear. *Proc. Roy. Soc. London A*, **225**, 49–63.

Bennett, S.J. and **Best, J.L.** (1995) Mean flow and turbulence structure over fixed, two-dimensional dunes: implications for sediment transport and bedform stability. *Sedimentology*, **42**, 491–513.

Best, J. and **Kostaschuk, R.** (2002) An experimental study of turbulent flow over a low-angle dune. *J. Geophys. Res.*, **107**, 3135. doi:10.1029/2000JC000294.

Bradley, J.V. (1968) *Distribution-Free Statistical Tests*. Prentice-Hall Inc, Englewood Cliffs, NJ.

Bradley, R.W., **Venditti, J.G.**, **Kostaschuk, R.A.**, **Church, M.**, **Hendershot, M.** and **Allison, M.A.** (2013) Flow and sediment suspension events over low angle dunes: Fraser Estuary, Canada. *J. Geophys. Res. Earth Surf.*, **118**. doi:10.1002/jgrf.20118.

ten Brinke, W.B.M., **Wilbers, A.W.E.** and **Wesseling, C**. (1999) Dune growth, decay and migration rates during a large-magnitude flood at a sand and mixed sand–gravel bed in the Dutch Rhine River System. *Fluvial Sedimentol.* **VI**, 15–32.

Carling, P.A., **Gölz, E.**, **Orr, H.G.** and **Radecki-Pawlik, A.** (2000a) The morphodynamics of fluvial sand dunes in the River Rhine near Mainz, Germany, Part I: sedimentology and morphology. *Sedimentology*, **47**, 227–252.

Carling, P.A., **Williams, J.J.**, **Gölz, E.** and **Kelsey, A.D.** (2000b) The morphodynamics of fluvial sand dunes in the River Rhine, near Mainz, Germany II. Hydrodynamics and sediment transport. *Sedimentology*, **47**, 253–278.

Coleman, S.E., **Nikora, V.I.**, **McLean, S.R.**, **Clunie, T.M.**, **Schicke, T.** and **Melville, B.W.** (2006) Equilibrium hydrodynamics concept for developing dunes. *Phys. Fluids*, **18**, 105104. doi:10.1063/1.23583332.

Dalrymple, R.W. and **Rhodes, R.N.** (1995) Estuarine dunes and bars. In: *Geomorphology and Sedimentology of Estuaries*. (Ed. G.M.E. Perillo), pp. 359–422. Elsevier, Amsterdam.

Dashtgard, S.E., **Venditti, J.G.**, **Hill, P.R.**, **Sisulak, C.F.**, **Johnson, S.M.** and **De La Croix, A.D.** (2012) Sedimentation across the tidal-fluvial transition in the Lower Fraser River, Canada. *Sed. Rec.*, **10**, 4–9.

Davis, R.A. and **Flemming, B.W**. (1991) Time-series study of mesoscale tidal bedforms, Martens Plate, Wadden Sea, Germany. In: *Clastic Tidal Sedimentology* (Eds D.G. Smith,

G.E. Reinson, B.A. Zaitlin and R.A. Rahmani), *Can. Soc. Petrol. Geol. Spec. Publ.*, **16**, 275–282.

Fernandez, R., **Best, J.** and **López, F.** (2006) Mean flow, turbulence structure, and bed form superimposition across the ripple-dune transition. *Water Resour. Res.*, **42**, W05406. doi:10.1029/2005WR004330.

Gabel, S.L. (1993) Geometry and kinematics of dunes during steady and unsteady flows in the Calamus River, Nebraska, USA. *Sedimentology*, **40**, 237–269.

Holmes, R.R. and **Garcia, M.H.** (2008) Flow over bedforms in a large sand-bed river: a field investigation. *J. Hydraul. Res.*, **46**, 322–333. doi:10.3826/jhr.2008.3040.

Hunter, R.E. and **Kocurek, G.** (1986) An experimental study of subaqueous slipface deposition. *J. Sed. Petrol.*, **56**, 387–394.

Johns, B., **Soulsby, R.L.** and **Chesher, T.J.** (1990) The modelling of sandwave evolution resulting from suspended and bedload transport of sediment. *J. Hydraul. Res.*, **28**, 355–374.

Julien, P.Y., **Klaassen, G.J.**, **Ten Brinke, W.B.M.** and **Wilbers, A.W.E.** (2002) Case study: bed resistance of Rhine River during the 1998 flood. *J. Hydraul. Eng.*, **128**, 1042–1050.

Kleinhans, M.G. (2004) Sorting in grain flows at the lee side of dunes. *Earth Sci. Rev.*, **65**, 75–102.

Kostaschuk, R. (2000) A field study of turbulence and sediment dynamics over subaqueous dunes with flow separation. *Sedimentology*, **47**, 519–531.

Kostaschuk, R. (2005) Sediment transport mechanics and dune morphology. In: *River, Coastal and Estuarine Morphodynamics: RCEM 2005* (Eds G. Parker and M. Garcia), pp. 795–803. Taylor and Francis, London.

Kostaschuk, R. (2006) Sediment transport mechanics and subaqueous dune morphology. In: *River, Coastal and Estuarine Morphodynamics* (Eds G. Parker and M. Garcia), pp. 795–801. Taylor and Francis, London.

Kostaschuk, R. and **Best, J**. (2005) Response of sand dunes to variations in tidal flow: Fraser River Estuary, Canada. *J. Geophys. Res.*, **110**, F04S04. doi:10.1029/2004JF000176.

Kostaschuk, R.A. and **Ilersich, S.A.** (1995) Dune geometry and sediment transport: Fraser River, British Columbia. In: *River Geomorphology* (Ed. E.J. Hickin), pp. 19–36. John Wiley and Sons, Chichester.

Kostaschuk, R.A. and **Luternauer, J.L.** (1989) The role of the salt wedge in sediment resuspension and deposition: Fraser River Estuary, Canada. *J. Coastal Res.*, **5**, 93–101.

Kostaschuk, R.A. and **Villard, P.V.** (1996) Flow and sediment transport over large subaqueous dunes: Fraser River, Canada. *Sedimentology*, **43**, 849–863.

Kostaschuk, R.A. and **Villard, P.V.** (1999) Turbulent sand suspension over dunes. *Int. Assoc. Sedimentol. Spec. Publ.*, **28**, 3–13.

Kostaschuk, R.A., **Church, M.A.** and **Luternauer, J.L.** (1989) Bedforms, bed material, and bedload transport in a salt-wedge estuary: Fraser River, British Columbia. *Can. J. Earth Sci.*, **26**, 1440–1452.

Kostaschuk, R., **Shugar, D.H.**, **Best, J.L.**, **Parsons, D.R.**, **Lane, S.N.**, **Hardy, R.** and **Orfeo, O.** (2009) Suspended sediment transport and deposition over a dune: Río Paraná, Argentina. *Earth Surf. Proc. Land.*, **34**, 1605–1611.

Leeder, M.R. (1983) On the interactions between turbulent flow, sediment transport and bedform mechanics in channelized flows. *Int. Assoc. Sedimentol. Spec. Publ.*, **6**, 5–18.

Lyn, D.A. (1993) Turbulence measurements in open-channel flow over bedforms. *J. Hydraul. Eng.*, **119**, 306–326.

McLaren, P. and **Ren, P**. (1995) *Sediment Transport and its Environmental Implications in the Lower Fraser River and Fraser Delta*. Environment Canada, Vancouver, BC. DOE FRAP 199-03.

McLean, S.R., **Nelson, J.M.** and **Wolfe, S.R.** (1994) Turbulence structure over two-dimensional bedforms: implications for sediment transport. *J. Geophys. Res.*, **99**, 12729–12747.

McLean, D.G., **Church, M.A.** and **Tassone, B.** (1999) Sediment transport along lower Fraser River. 1. Measurements and hydraulic computations. *Water Resour. Res.*, **35**, 2533–2548.

Nelson, J.M., **McLean, S.R.** and **Wolfe, S.R.** (1993) Mean flow and turbulence over two-dimensional bedforms. *Water Resour. Res.*, **29**, 3935–3953.

Nittrouer, J.A., **Allison, M.A.** and **Campanella, R.** (2008) Bedform transport rates for the lowermost Mississippi River. *J. Geophys. Res.*, **113**, F03004. doi:1029/2007JF000795.

Paarlberg, A.J., **Dohmen-Janssen, C.M.**, **Hulscher, S.J.M.H.** and **Termes, P.** (2007) A parameterization of flow separation over subaqueous dunes. *Water Resour. Res.*, **43**, W12417. doi:10.1029/2006WR005425.

Pailha, M. and **Pouliquen, O.** (2009) A two-phase flow description of the initiation of underwater granular avalanches. *J. Fluid Mech.*, **633**, 115–135.

Pailha, M., **Nicolas, M.** and **Pouliquen, O.** (2008) Initiation of underwater granular avalanches: influence of the initial volume fraction. *Phys. Fluids*, **20**, 111701.

Parsons, D.R., **Best, J.L.**, **Orfeo, O.**, **Hardy, R.J.**, **Kostaschuk, R.** and **Lane, S.N.** (2005) Morphology and flow fields of three-dimensional dunes, Rio Paraná, Argentina: results from simultaneous multibeam echo sounding and acoustic Doppler current profiling. *J. Geophys. Res.*, **110**, F04S03. doi:10.1029/2004JF000231.

Pretious, E.S. and **Blench, T**. (1951) Final report on special observations on bed movement in the lower Fraser River at Ladner Reach during the 1950 freshet. National Research Council of Canada, Fraser River Model Project.

Reson Inc. (2009) SeaBat 7101 High-Resolution Multibeam Echosounder System, Operator's Manual. Denmark, 168 pp.

Reynolds, O. (1886) Dilatancy. *Nature*, **33**, 429–430.

Rhodes, R.N. (1992) Hydrodynamics and the morphology, migration and structure of subaqueous dunes, Minas Basin, Canada. M.Sc. Thesis, Queen's University, Kingston, ON.

Roden, J.E. (1998) The sedimentology and dynamics of mega-dunes, Jamuna River, Bangladesh. Ph.D. Thesis, Department of Earth Science, University of Leeds, Leeds.

Shugar, D.H., **Kostaschuk, R.**, **Best, J.L.**, **Parsons, D.R.**, **Lane, S.N.**, **Orfeo, O.** and **Hardy, R.** (2010) On the relationship between flow and suspended sediment transport over the crest of a sand dune, Rio Parana, Argentina. *Sedimentology*, **57**, 252–272.

Smith, J.D. and **McLean, S.R.** (1977) Spatially averaged flow over a wavy surface. *J. Geophys. Res.*, **82**, 1735–1746.

Sorby, H.C. (1852) On the oscillations of the currents drifting the sandstone beds of the southeast of Northumberland, and on the general direction in the coalfield in the neighbourhood of Edinburgh. *Proc. Yorks. Geol. Soc.*, **3**, 232–240.

Sorby, H.C. (1908) On the application of quantitative methods to the study of the structure and history of rocks. *Q. J. Geol. Soc. London*, **64**, 171–232.

Soulsby, R.L., **Atkins, R.**, **Waters, C.B.** and **Oliver, N**. (1991) Field measurements of suspended sediment over sandwaves. In: *Sand Transport in Rivers, Estuaries, and Sea* (Eds R.L. Soulsby and R.E. Bettess), pp. 155–162. A.A. Balkema, Brookfield, VT.

Southard, J.B. and **Boguchwal, L.A.** (1990a) Bed configurations in steady unidirectional water flow part 1. Scale model study using fine sands. *J. Sed. Res.*, **60**, 649–657.

Southard, J.B. and **Boguchwal, L.A.** (1990b) Bed configurations in steady unidirectional water flow part 2. Synthesis of flume data. *J. Sed. Petrol.*, **60**, 658–679.

Terwindt, J.H.J. and **Brouwer, M.J.N.** (1986) The behaviour of intertidal sandwaves during neap-spring tide cycles and the relevance to paleoflow reconstructions. *Sedimentology*, **33**, 1–31.

Venditti, J.G. (2007) Turbulent flow and drag over fixed two-dimensional and three-dimensional dunes. *J. Geophys. Res. Earth Surf.*, **112**, F04008. doi:10.1029/2006JF000650.

Venditti, J.G. (2013) Bedforms in sand-bedded rivers. In: *Treatise on Geomorphology, Fluvial Geomorphology* (Eds J.F. Shroder (Editor-in-Chief) and E. Wohl (Volume Editor)), vol. 9, pp. 137–162. Academic Press, San Diego, CA.

Venditti, J.G. and **Bauer, B.O.** (2005) Turbulent flow over a dune: Green River, Colorado. *Earth Surf. Proc. Land.*, **30**, 289–304. doi:10.1002/esp.1142.

Venditti, J.G. and **Bennett, S.J.** (2000) Spectral analysis of turbulent flow and suspended sediment transport over fixed dunes. *J. Geophys. Res.*, **105**, 22035–22047.

Venditti, J.G., **Church, M.A.** and **Bennett, S.J.** (2005) Morphodynamics of small-scale superimposed sandwaves over migrating dune bedforms. *Water Resour. Res.*, **41**, W10423. doi:10.1029/2004WR003461.

Villard, P.V. and **Church, M.A.** (2003) Dunes and associated sand transport in a tidally influenced sand-bed channel: Fraser River, British Columbia. *Can. J. Earth Sci.*, **40**, 115–130.

Villard, P.V. and **Church, M.A.** (2005) Bar and dune development during a freshet: Fraser River Estuary, British Columbia, Canada. *Sedimentology*, **52**, 737–756.

Western Canada Hydraulic Laboratories Ltd (1977) Feasibility study, development of a forty-foot draft navigation channel, New Westminster to Sandheads. Unpublished report to Public Works Canada.

Wiberg, P.L. and **Nelson, J.M.** (1992) Unidirectional flow over asymmetric and symmetric ripples. *J. Geophys. Res.*, **97**, 12745–12761.

Wilbers, A.W.E. (2004) Prediction of bedform characteristics and bedform roughness in large rivers, Ph.D. thesis, Utrecht University., Utrecht.

Wilbers, A.W.E. and **ten Brinke, W.B.M.** (2003) The response of subaqueous dunes to floods in sand and gravel bed reaches of the Dutch Rhine. *Sedimentology*, **50**, 1013–1034.

Yalin, M.S. (1972) *Mechanics of Sediment Transport*. Pergamon Press, Oxford.

Yalin, M.S. and **Karahan, E.** (1979) Steepness of sedimentary dunes. *J. Hydraul. Div.*, **105**, 381–392.

Manuscript received 22 December 2014; revision accepted 18 September 2015